Influence of biogenic emissions from boreal forests on aerosol-cloud interactions

Petäjä, Tuukka

2022-01

Petäjä , T , Tabakova , K , Manninen , A , Ezhova , E , O'Connor , E , Moisseev , D , Sinclair , V , Backman , J , Levula , J , Luoma , K , Virkkula , A , Paramonov , M , Räty , M , Äijälä , M , Heikkinen , L , Ehn , M , Sipilä , M , Yli-Juuti , T , Virtanen , A , Ritsche , M , Hickmon , N , Pulik , G , Rosenfeld , D , Worsnop , D , Back , J , Kulmala , M & Kerminen , V-M 2022 , ' Influence of biogenic emissions from boreal forests on aerosol-cloud interactions ' , Nature Geoscience , vol. 15 , no. 1 , pp. 42-+ . https://doi.org/10.1038/s41561-021-00876-0

http://hdl.handle.net/10138/345452
https://doi.org/10.1038/s41561-021-00876-0

other
acceptedVersion

Influence of biogenic emissions from boreal forests on aerosol-cloud interactions

T. Petäjä[1,2*], K. Tabakova[1], A. Manninen[1,3], E. Ezhova[1], E. O'Connor[3,4], D. Moisseev[1,3], V.A. Sinclair[1], J. Backman[1,3], J. Levula[1], K. Luoma[1], A. Virkkula[1,2,3], M. Paramonov[1,3], M. Räty[1], M. Äijälä[1], L. Heikkinen[1], M. Ehn[1], M. Sipilä[1], T. Yli-Juuti[5], A. Virtanen[5], M. Ritsche[6], N. Hickmon[6], G. Pulik[7], D. Rosenfeld[7], D.R. Worsnop[1,8], J. Bäck[9], M. Kulmala[1,2,10,11] and V.-M. Kerminen[1]

[1]Institute for Atmospheric and Earth System Research (INAR) / Physics, Faculty of Science, University of Helsinki, Finland
[2]Joint International Research Laboratory of Atmospheric and Earth System Sciences (JirLATEST), School of Atmospheric Sciences, Nanjing University, Nanjing, China
[3]Finnish Meteorological Institute, Helsinki, Finland
[4]University of Reading, UK
[5]Department of Applied Physics, University of Eastern Finland, Kuopio, Finland
[6]Argonne National Laboratory, Lemont, IL, USA
[7]Institute of Earth Sciences, The Hebrew University of Jerusalem, Jerusalem, Israel.
[8]Aerodyne Research Inc., Billerica, MA, USA
[9]Institute for Atmospheric and Earth System Research (INAR) / Forest Sciences, Faculty of Agriculture and Forestry, University of Helsinki, Finland
[10]Aerosol and Haze Laboratory, Beijing Advanced Innovation Center for Soft Matter Sciences and Engineering, Beijing University of Chemical Technology (BUCT), Beijing, China
[11]Faculty of Geography, Lomonosov Moscow State University, Moscow, Russia

[*]Correspondence to: tuukka.petaja@helsinki.fi

Abstract

Boreal forest acts as a carbon sink and contributes to the formation of secondary organic aerosols via emission of aerosol precursor compounds. However, these influences on the climate system are poorly quantified. Here we show direct observational evidence that aerosol emissions from the boreal forest biosphere influence warm cloud microphysics and cloud-aerosol interactions in a scale-dependent and highly dynamic manner. Analyses of in-situ and ground-based remote sensing observations from the SMEAR II station in Finland, conducted over eight months in 2014, reveal significant increases in aerosol load over the forest one to three days after aerosol-poor marine air enters the forest environment. We find that these changes are consistent with secondary organic aerosol formation and, together with water vapor emissions from evapotranspiration, are associated with changes in the radiative properties of warm, low-level clouds. The feedbacks between boreal forest emissions and aerosol-cloud interactions and the highly dynamic nature of these

interactions in air transported over the forest over timescales of several days suggest boreal forests have the potential to mitigate climate change on a continental scale. Our findings suggest that even small changes in aerosol precursor emissions, whether due to changing climatic or anthropogenic factors, may substantially modify the radiative properties of clouds in moderately polluted environments.

Interactions between aerosol particles and clouds constitute a key uncertainty in our knowledge of the Earth's energy budget and anthropogenic climate[1]. The aerosol-induced radiative forcing of warm clouds results from changes in the cloud droplet number concentration, cloud liquid water path and fractional cloud cover[2]. There is ample evidence that aerosol particles are capable of modifying cloud microphysical properties, whereas much less is known about the responses of cloud cover or liquid water path to aerosol perturbations[3-11]. Very little is known about how cloud properties are affected by dynamic changes in an ambient aerosol particle population over time and space. Here, we provide an observation-based estimate of the effects that emissions from a boreal forest biosphere have on the time evolution of the aerosol population, warm cloud microphysics, aerosol-cloud interactions and precipitation. Our data set represents clean maritime air that is transformed into continental air, addressing the specific need to reduce the large uncertainties in the aerosol radiative forcing caused by natural aerosols[12].

Boreal forests, situated in a circumpolar belt in the Northern latitudes[13], are among the most active areas of atmospheric new particle formation (NPF)[14-16]. The particles formed by NPF in this environment grow in size during atmospheric transport (Fig. 1) and, for air masses originating from clean areas outside the winter period, a vast majority of this growth can be attributed to biogenic aerosol precursor emissions from the forest, their atmospheric oxidation and consequent condensation during the air mass transport[17-20]. These processes produce new cloud condensation nuclei (CCN)[15,21] and, via activation, these CCN form cloud droplets that can have large radiative effects[22,23]. Boreal forests provide, therefore, an ideal locale to investigate aerosol-cloud interactions in an evolving natural aerosol system affected to only a minor extent by anthropogenic emissions[24].

We conducted intensive observations with comprehensive in-situ and ground-based remote sensing instrumentation during Biogenic Aerosols – Effects on Clouds and Climate, BAECC[25] campaign for over 8 months in 2014, which complemented the long-term aerosol observations at Station for Measuring Ecosystem-Atmosphere Relations (SMEAR II)[26] in Hyytiälä, Finland (Fig. 1a). The *in-situ* aerosol and ground-based remote sensing instruments are presented in Methods section. We calculated a parameter "time over land" that is determined from back-trajectory analysis (See Methods section for details). This parameter corresponds to the exposure time of an air mass to the boreal forest environment prior to being measured at the site. We concentrated on air masses originating from the north-west direction in order to minimize the influence of anthropogenic emissions[24,37], (see also the discussion in the Methods section). We calculated medians of *in-situ* data

measured within 1 hour of the air mass arrival time for every time over land value. After classifying the chosen data as a function of time over land, we found that the aerosol number size distribution evolves considerably during its residence time over the biosphere (Figures 1b, 1c), consistent with earlier analyses[17].

Time evolution of the in situ-measured aerosol population

The following synthesis for the time evolution of the *in situ*-measured aerosol population emerges: between the 20 and 75 hours of air mass transport time over land, the aerosol mass concentration increases by a factor of 3–4 (Table 1). This mass consists largely of organic material (Fig. 2a), especially at longer transport time over land, and is dominated by oxidized organic compounds indicative of secondary organic aerosol formation[28-30], see also Extended Data Fig 2).

The particle number size distribution is initially dominated by nucleation mode particles (diameter <25 nm), and later by Aitken mode particles (25–100 nm) with a growing tail into the accumulation mode (>100 nm, Figure 1b). The simultaneous increase of both mass and mean size of the aerosol population makes it optically more active, which is reflected by the increasing aerosol scattering and backscatter coefficients (Fig. 2b and 2c, Table 1), both by a factor of about 5.5. The aerosol backscatter fraction decreases (Extended Data Fig. 3) with increasing time over land because, compared with smaller particles, larger particles scatter more efficiently into the forward direction. CCN concentrations (at water vapor supersaturations of 0.1–0.5 %) increase by factors of 4.0 – 4.6 between 20 and 75 hours of air mass transport over land (Table 1, Fig. 3a). This increase is almost entirely due to the increasing particle size in the sub-100 size range, as the critical diameter for CCN activity at higher water vapor supersaturations changes little during the aerosol aging (Extended Data Fig. 4).

Aerosol particles in the boundary layer

High Spectral Resolution lidar (HSRL[31]) data expands *in situ* optical measurements vertically into the boundary layer (see Methods section). We found that the backscatter coefficient averaged for a 60 m layer (two HSRL range gates) at 200 m and at 500 m above ground level (a.g.l) increases by a factor of about 1.3 between the 20 and 75 hours of air mass transport time over land (Fig. 2d). Although based on a smaller dataset than *in situ* optical measurements, the increase of the backscatter coefficient aloft indicates that the changes in the time evolution of the aerosol population observed at ground level reflect those taking place throughout the lower boundary layer in air masses transported to our measurement site.

To complete the analysis, we derived cloud droplet number concentrations (CDNC) using ground-based remote sensing (see Methods section). We restricted our analysis to non-precipitating, low-level liquid clouds (cloud bases below 2000 m) in order to minimize the potential effect of rain and ice-forming processes on cloud microphysics, and because such clouds are more likely to interact with boundary-layer aerosol particles than mid- or higher-level clouds. For this cloud type, the median CDNC almost doubles between the 20 and 75 hours of air mass transport time over land (Figure 3b, Table 1). A similar increase can be observed in the cloud liquid water path (LWP), plausibly as a result of increasing specific humidity due to evapotranspiration from the forest biosphere during air mass transport to the site (Extended Data Fig. 5). In general terms, the albedo of a cloud is closely tied with its optical thickness, τ, which can be approximated to be proportional to $LWP^{5/6} \times CDNC^{1/3}$ for adiabatic liquid clouds[32,33]. The enhancement in CDNC and LWP observed in our dataset could lead to a corresponding factor of 2 increase in τ between the 20 and 75 hours of air mass transport over land. To complement our ground-based observations, we derived CCN concentrations from satellite data[34]. As an example, the result of a case during August 17, 2014 is presented in Figure 3c, see also Extended Data Fig 6). The spatial pattern of CCN concentrations shows that the CCN concentrations are higher in-land than they are at the coast line. This snapshot analysis is consistent with our ground-based in-situ and remote sensing data. Overall, these observations are indicative of major changes in cloud radiative properties when clean air is transported over a boreal forest and is subsequently modified by interactions with the forest biosphere. The overall radiative effect from aerosol-cloud interactions is likely to experience changes of similar magnitude, as we found no systematic change in the cloud fraction as a function of time over land (Extended Data Fig. 7).

Besides the influence of aerosols on clouds discussed above, clouds can influence the aging of an aerosol particle population as well. For example, non-precipitating cloud processing and associated cloud water chemistry create a bimodal particle number size distribution with a clear minimum slightly below 100 nm in remote marine air[35,36]. We observed signs of non-precipitating cloud processing after about 30–40 hours of time over land, and the resulting minimum in the particle number distribution was quite evident at longer air mass transport times (Fig. 1c). Precipitation scavenging is usually thought as the main removal mechanisms for atmospheric aerosol particles[37, 38]. In our data set, the probability and intensity of rain show considerable variability with a tendency to increase with an increasing time over land (Extended Data Fig. 7). The observed behavior of extensive aerosol properties (Figs. 1–3), CDNC (Fig. 3b) and LWP (Extended Data Fig. 5) suggests that secondary aerosol formation clearly dominates over aerosol losses by precipitation scavenging for air mass transport times of at least 70–80 hours over land.

Implications for aerosol-cloud interactions

Interestingly, during the approximately 75h time period we are able to observe the whole chain of processes starting from condensable vapor production associated with emissions from the biosphere, continuing with atmospheric new particle formation and growth, and eventually leading to additional CCN and cloud droplets, with simultaneous signs of cloud processing, initiation of precipitation and precipitation scavenging of the aerosol population. Considering a typical air mass movement velocity, and distance of the observations to the coastline, the corresponding spatial scale for this chain of processes is approximately 1 million km^2. This is the required temporal and spatial scale to study aerosol impacts on cloud properties and precipitation in the boreal environment.

Figure 4 summarizes schematically how a boreal forest environment influences aerosols and clouds, and how the time evolution of both aerosol and cloud properties evolve together when being affected by forest biosphere emissions. Considerable changes were observed in both aerosol and cloud properties, as well as in signatures of aerosol-cloud interactions, for up to 3 days of air mass transport over the forest. The highly dynamic nature of this system has several important consequences that probably hold for many other continental environments which emit aerosol precursor vapors or primary aerosol particles. First, there is no static natural background state for continental aerosol particle populations, nor for cloud microphysical properties, unless the environmental system under consideration is large enough; in our case several hundreds of kilometers in length. Second, even small changes in aerosol precursor emissions due to changing climatic conditions[3], or due to anthropogenic influences[39,40], may substantially affect the radiative and precipitating properties of clouds in moderately-polluted environments. Finally, while it is generally accepted that the behavior of atmospheric cloud systems depends on a wide variety of temporal and spatial scales[2,41], our results imply that such a scale-dependency is also a characteristic feature of aerosol-cloud interactions involving low clouds over moderately-polluted regions affected by surface emissions. Our findings call for similar studies in other continental environments, and pose challenges not only for studies of aerosol-cloud interactions, but also when using atmospheric aerosol or cloud data for model evaluation or when investigating feedback mechanisms between the atmosphere and biosphere.

Acknowledgments: The work was supported by Academy of Finland via Center of Excellence in Atmospheric Sciences (project no. 272041), Flagship program for Atmospheric and Climate Competence Center (ACCC, 337549, 337552, 337550) and grants 317380, 320094 and 334792, 328290, 302958, 325656, 316114, 325647, 325681 and 341271, European Research Council Advanced Grants (227463-ATMNUCLE, 742206-ATM-GTP,) and Starting Grants (638703-COALA, 714621-GASPARCON), the Arena for the gap analysis of the existing Arctic Science Co-Operations (AASCO) funded by Prince Albert Foundation Contract No 2859, and "Quantifying carbon sink, CarbonSink+ and their interaction with air quality" INAR project funded by Jane and

Aatos Erkko Foundation. This work was partly supported by the Office of Science (BER), U.S. Department of Energy via BAECC (Petäjä, DE-SC0010711), BAECC-SNEX (Moisseev), European Commission via projects This project has received funding from the European Union's Horizon 2020 research and innovation program under grant agreement No. 821205 (Understanding and reducing the long-standing uncertainty in anthropogenic aerosol radiative forcing, FORCeS) and ACTRIS, ACTRIS-TNA, ACTRIS2, ACTRIS-IMP, BACCHUS, eLTER, ICOS, PEGASOS and Nordforsk via Cryosphere-Atmosphere Interactions in a Changing Arctic Climate, CRAICC, The BAECC SNEX was also supported by NASA Global Precipitation Measurement (GPM) Mission ground validation program. The deployment of AMF2 to Hyytiälä was enabled and supported by ARM. Argonne National Laboratory's work was supported by the U.S. Department of Energy, Assistant Secretary for Environmental Management, Office of Science and Technology, under contract DE-AC02-06CH11357. The ground-based data used in this study were obtained from the Atmospheric Radiation Measurement (ARM) user facility, managed by the Office of Biological and Environmental Research for the U.S. Department of Energy Office of Science. We acknowledge ACTRIS for providing the products derived from the ground-based data in this study, which were produced by the Finnish Meteorological Institute, and are available for download from https://cloudnet.fmi.fi/. The authors gratefully acknowledge the support of AMF2, SMEAR2 and the BAECC community for their support in initiating the BAECC campaign, its implementation, operation, data analysis and interpretation. The authors are grateful for the four anonymous referees for their comments which improved the paper considerably.

Competing interests:

The authors declare no competing interests.

Corresponding Author: Tuukka Petäjä, tuukka.petaja@helsinki.fi

238 **Tables:**
239
240 **Table 1:** Concentrations of aerosol total mass, organic aerosol mass and CCN, as well as
241 the scattering and backscatter coefficient at 20 and 75 hours of air mass transport time over
242 land, along with the enhancement factor between these two transport times. In case of the
243 cloud droplet number concentration (CDNC), the results were averaged over transport
244 times of 20–50 and 50–80 h over land.
245

Type of observation	**Parameter**	**Transport time over land = 20 h**	**Transport time over land = 75 h**	**Enhancement factor**
Aerosol in-situ	Aerosol mass concentration (μg m-3)	1.0	3.5	3.5
Aerosol in-situ	Organic aerosol mass concentration (μg m^{-3})	0.3	2.5	8.3
Aerosol in-situ	Cloud condensation nuclei concentration at Sc = 0.1 %, 0.2 %, 0.3 % and 0.5 % (cm^{-3})	40 105 155 840	180 490 610 980	4.5 4.6 3.9 1.2
Aerosol in-situ	Scattering coefficient (Mm^{-1})	3.1	17.4	5.6
Aerosol in-situ	Backscattering coefficient (Mm^{-1})	0.45	2.4	5.3
Aerosol ground-based remote sensing	Backscattering coefficient at 200 m and 500 m a.g.l. (m sr^{-1})	5.6 * 10^{-7} 5.6 * 10^{-7}	7.25 * 10^{-7} 7.25 * 10^{-7}	1.3 1.3
Cloud ground-based remote sensing	CDNC for clouds with cloud base height < 1200 m and < 2000 m (cm^{-3})	490 270	650 600	1.3 2.2

246
247

Figures and Figure Captions:

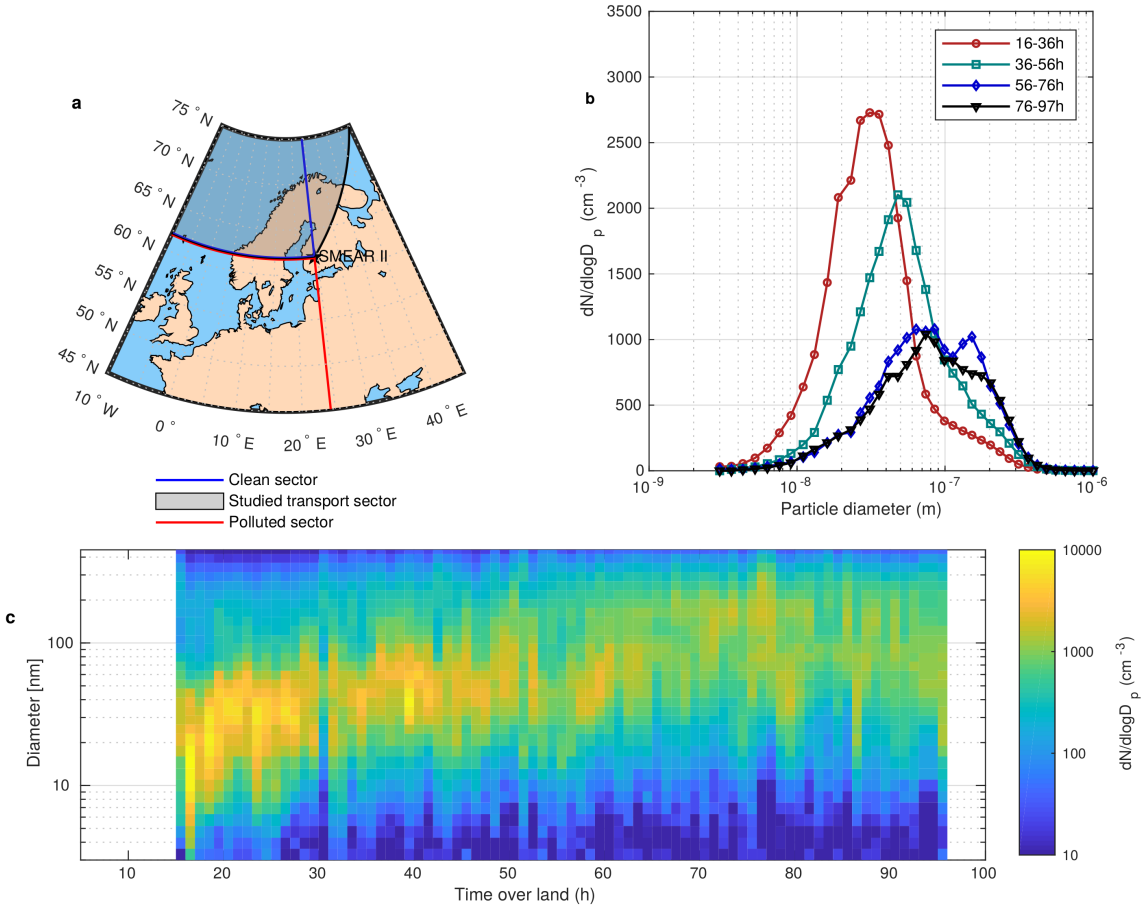

Fig. 1. Time evolution of the particle number size distribution. a. Location of the SMEAR II station in Hyytiälä, Finland, and the three air mass transport sectors discussed in this paper. Most of the analysis discussed in this paper is based on air masses residing in the studied transport sector (STS, see Methods). **b.** Median particle number size distributions for different time-over-land classes in STS. **c.** Evolution of the particle number size distribution as a function of time over land for air masses in STS. Atmospheric new particle formation (NPF) is frequent at short air mass transport times over the boreal forest region (See Fig. Extended Data Fig. 1), leading to a pronounced mode of particles in the sub-50 nm size range. Growth of pre-existing particles dominates over NPF at longer transport times over land, increasing the mean size of the particle population. At the longest transport times over land, the bimodality of the particle population and the pronounced Hoppel-minimum[32] between the Aitken and accumulation mode indicate non-precipitating cloud processing.

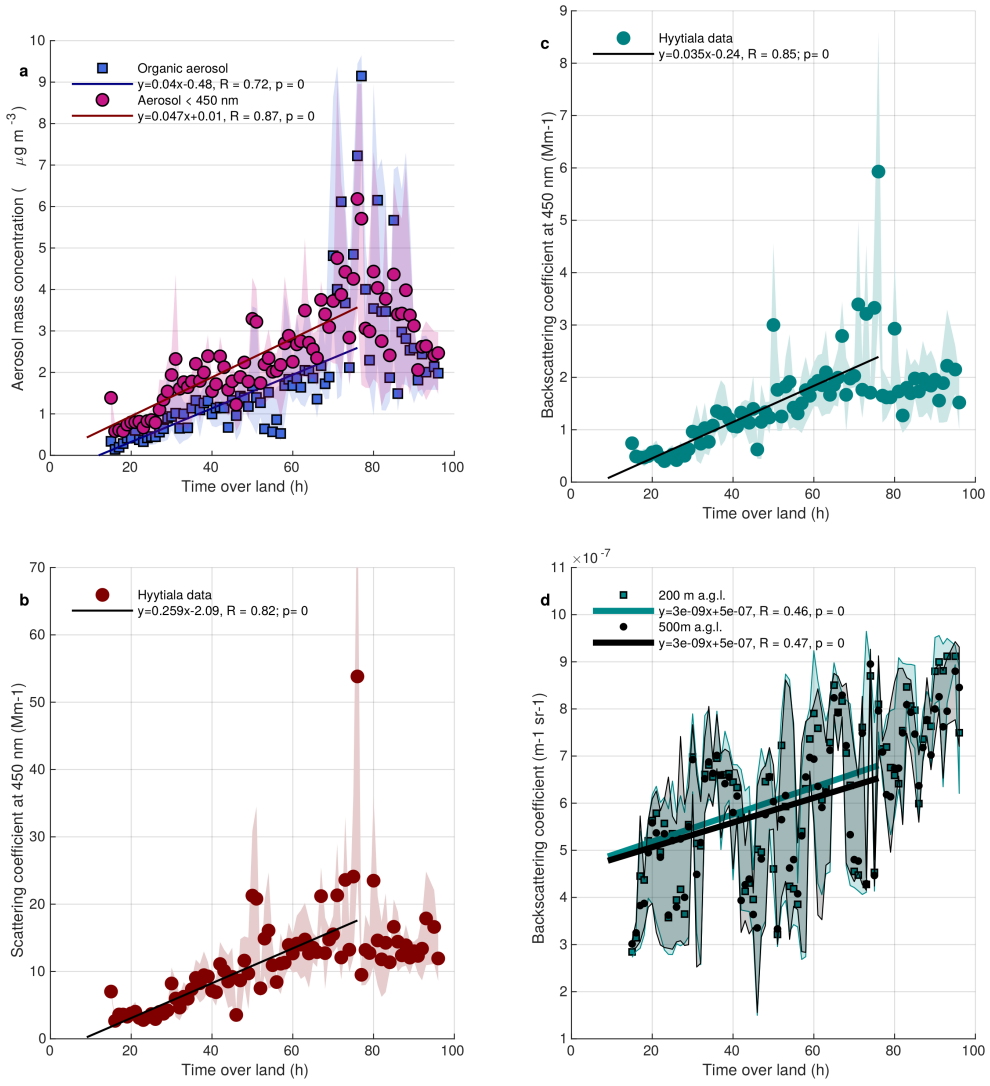

Fig. 2 Time evolution of the particle mass concentration and optical properties. a. Total aerosol mass concentration below below 450 nm estimated from the measured DMPS volume size distribution assuming an aerosol density of 1.5 g cm^{-3}, and organic mass concentration measured with aerosol mass spectrometry. **b.** In-situ measured scattering coefficient. **c.** In-situ measured backscattering coefficient. **d.** Backscattering coefficient retrieved with the HSRL lidar at 200 m and 500 m above ground level. The increase in backscatter coefficient aloft is consistent with the in-situ data. Shaded areas in the panels represent 25th to 75th percentile ranges. Solid lines show weighted least-squares fit to the data up to 75 h time over land. Regression equations, correlation coefficients and p-values are shown in legends. In summary, results are consistent with the assumption that the residence time over land affects the aerosol population throughout the lower boundary layer.

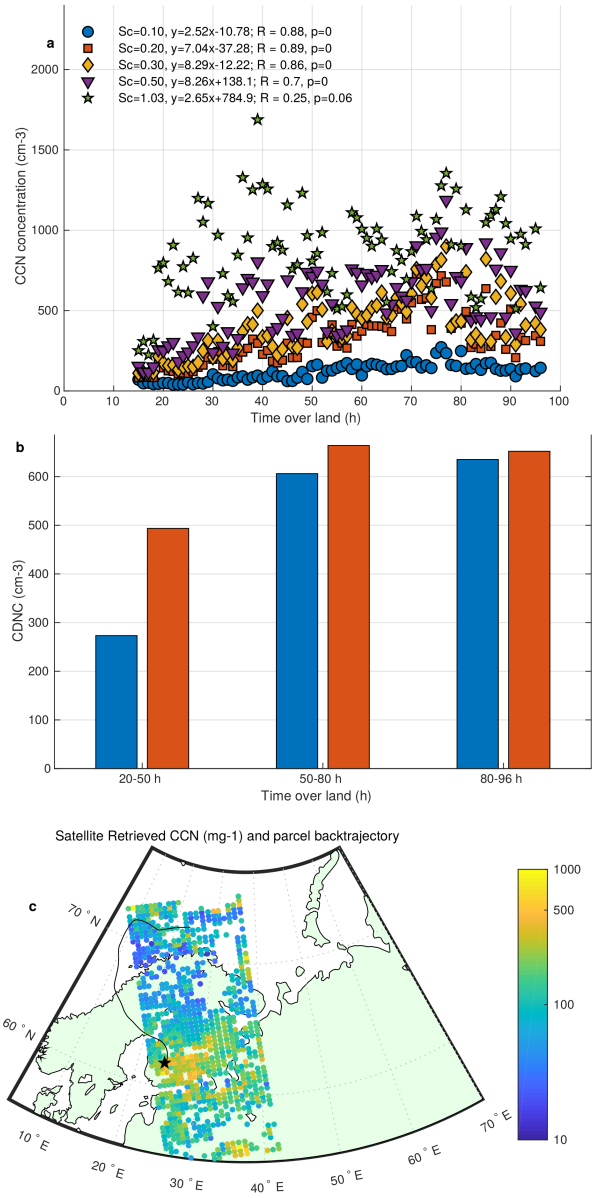

Fig. 3 Cloud-related variables. a. CCN number concentration at different water vapor supersaturations (Sc) as a function of time over land. The legend shows the regression equations of weighted least-squares fit to the data up to 75 h time over land, correlation coefficients and p-values. **b.** Median retrieved cloud droplet number concentration (CDNC) in liquid single-layer, non-precipitating clouds. The data were binned according to the time that an air parcel spent over land: 20–50, 50–80 and 80–96 hours. The two colors differentiate between the cases with the cloud base located below 2000 m and 1200 m. **c.** A map of CCN concentrations determined from satellite for an exemplary case study on August 17, 2014 when the air masses arrive at Hyytiälä from the Arctic Ocean. The satellite-derived CCN concentrations show a substantial increase from the coast-line to inland.

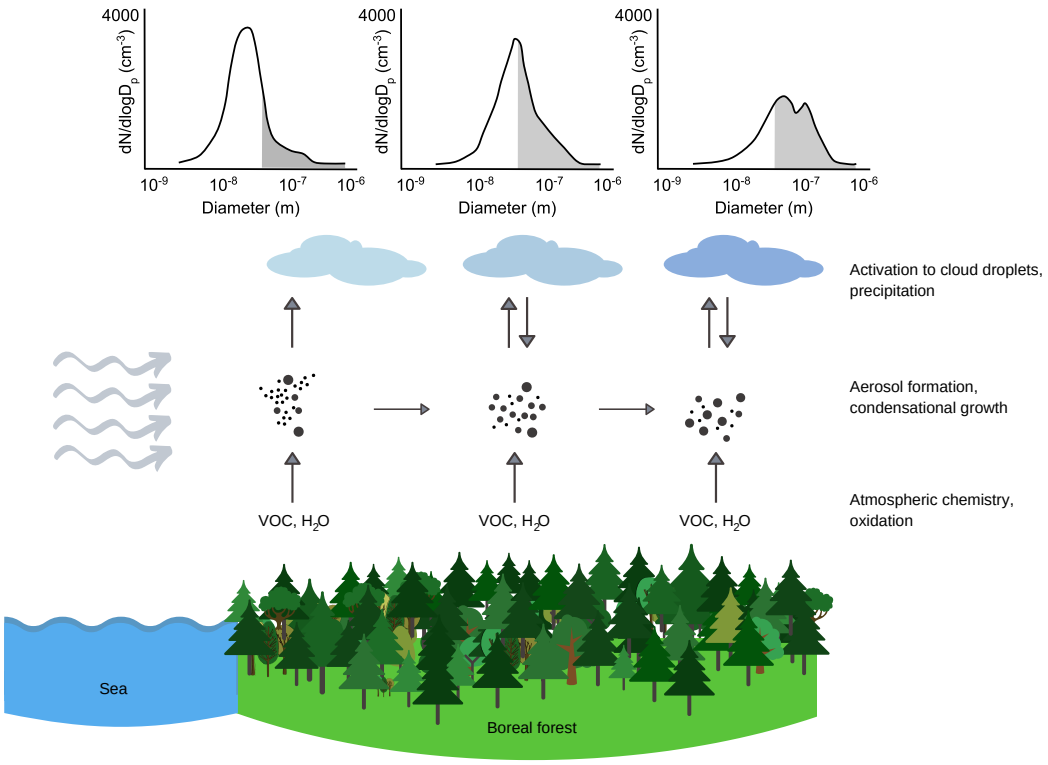

Fig. 4 Schematic representation of processes affecting aerosols and clouds during an air mass transport over boreal forests. When initially clear air enters the boreal forest environment (left part of the figure), it begins accumulating aerosol precursors together with water vapor from the forest biosphere. This leads to cloud formation, probably relatively soon after the air mass enters the forest environment[45]. At longer air mass transport times over the forest (right part of the figure), the accumulating water vapor makes the existing clouds optically thicker, and thereby more reflective to incoming solar radiation; eventually leading to precipitation. Atmospheric oxidation of biogenic aerosol precursors vapors initiates a sequence of processes starting from NPF and secondary aerosol formation and ending with increased CCN and cloud droplet number concentrations. This further enhances cloud reflectivity at longer air mass transport times over the forest, while at the same time delaying the onset of precipitation expected from accumulating water vapor.

References:

[1] Boucher, O. et al. Clouds and Aerosols in: Climate Change 2013: The Physical Science Basis. Contribution of Working Group I to the Fifth Assessment Report of the Intergovernmental Panel on Climate Change, T. Stocker, et al. (Eds), Cambridge University Press. (2013).

[2] Rosenfeld, D. et al. Global observations of aerosol-cloud-precipitation-climate interactions. *Rev. Geophys.* **52**, 750-808 (2014).

[3] Twohy, C.H. et al. Impacts of aerosol particles on the microphysical and radiative properties of stratocumulus clouds over the southeast Pacific Ocean. *Atmos. Chem. Phys.* **13**, 2541-2562 (2013).

[4] Goren, T. & Rosenfeld, D. Extensive closed cell marine stratocumulus downwind of Europe – A large aerosol cloud mediated radiative effect or forcing? *J. Geophys. Res. Atmos.* **120**, 6098-6116 (2015).

[5] Liu, Y. et al. Analysis of aerosol effects on warm clouds over the Yangtze River Delta from multi-sensor satellite observations. *Atmos. Chem. Phys.* **17**, 5623-5641 (2017).

[6] Malavelle, F.F. et al. Strong constraints on aerosol-cloud interactions from volcanic eruptions. *Nature* **546**, 485-491 (2017).

[7] Lu, Z. et al. Biomass smoke from southern Africa can significantly enhance the brightness of stratocumulus over the southeastern Atlantic Ocean. *Proc. Natl. Acad. Sci.* **115**, 2924-2929 (2018).

[8] Ross, A.D. et al. Exploring the first aerosol indirect effect over Southeast Asia using a 10-year collocated MODIS, CALIOP, and model dataset. *Atmos. Chem. Phys.* **18**, 12747-12764 (2018).

[9] Gryspeerdt, E. et al. Constraining the aerosol influence on cloud liquid water path. *Atmos. Chem. Phys.,* **19**, 5331-5347 (2019).

[10] Mülmentstädt, J. et al. Reducing the aerosol forcing uncertainty using observational constraints on warm rain processes. *Sci. Adv.*, **6**, eaaz6733 (2020).

[11] Bellouin, N. et al. Bounding global aerosol radiative forcing of climate change. *Rev. Geophys.*, **58**, doi.org/10.1029/2019RG000660 (2020).

[12] Carslaw, K.S. et al. Large contribution of natural aerosols to uncertainty in indirect forcing. *Nature* **503**, 67-71 (2013).

[13] Bonan, G.P. Forests and climate change: forcings, feedbacks, and the climate benefits of forests. *Science* **320**, 1444-1449 (2008).

[14] Kulmala, M. et al. Direct observations of atmospheric nucleation. *Science* **339**, 943-946 (2013).

[15] Paasonen, P. et al. Warming-induced increase in aerosol number concentration likely to moderate climate change. *Nature Geosci*. **6**, 438-442 (2013).

[16] Kerminen, V.-M. et al. Atmospheric new particle formation and growth: review of field observations. *Environ*. *Res*. *Lett*. **13**, 103003 (2018).

[17] Tunved, P. et al. High natural aerosol loading over boreal forests. *Science* **312**, 261–263 (2006).

[18] Riipinen, I. et al. The contribution of organics to atmospheric nanoparticle growth. *Nature Geosci*. **5**, 453-458 (2012).

[19] Ehn, M. et al. A large source of low-volatility secondary organic aerosol. *Nature* **506**, 476–479 (2014).

[20] Tröstl, J. et al. The role of low-volatility organic compounds in initial particle growth in the atmosphere. *Nature* **533**, 527-533 (2016).

[21] Pierce, J.R., Westerveld, D.M., Atwood, S.A., Barne, E.A., & Leaitch, W.R. New-particle formation, growth and climate-relevant particle production in Egbert, Canada: analysis of 1 year of size-distribution observations. *Atmos*. *Chem*. *Phys*. **14**, 8647-8663 (2014).

[22] Spracklen, D.V., Bonn, B. & Carslaw, K.S. Boreal forests, aerosol and the impacts on clouds and climate. *Phil*. *Trans*. *R*. *Soc*. *A*., doi:10.1098/rsta.2008.0201 (2008).

[23] Scott, C.E. et al. The direct and indirect radiative effects of biogenic secondary organic aerosol. *Atmos*. *Chem*. *Phys*. **14**, 447-470 (2014).

[24] Riuttanen, L., Hulkkonen, M., Dal Maso, M., Junninen, H. & Kulmala, M. Trajectory analysis of atmospheric transport of fine particles, SO_2, NO_x and O_3 to the SMEAR II station in Finland in 1996–2008. *Atmos*. *Chem*. *Phys*. **13**, 2153-2164 (2013).

[25] Petäjä, T. et al. BAECC, A field campaign to elucidate the impact of Biogenic Aerosols on Clouds and Climate. Bull. Am. Met. Soc. 97, 1909-1928 (2016).

[26] Hari, P. & Kulmala, M. Station for Measuring Ecosystem – Atmosphere Relations (SMEAR II). *Boreal Environ*. *Res*. **10**, 315-322 (2005).

[27] Petäjä, T. et al. Effects of SO_2 oxidation on ambient aerosol growth in water and ethanol vapours. *Atmos. Chem. Phys.* **5**, 767-779 (2005).

[28] Aiken, A.C. et al. O/C and OM/OC ratios of primary, secondary, and ambient organic aerosols with high-resolution time-of-flight aerosol mass spectrometry. *Environ. Sci. Technol.,* **42**, 4478-4485 (2008).

[29] Yatavelli, R.L.N et al. Estimating the contribution of organic acids to northern hemispheric continental organic aerosol. Geophys. Res. Lett., 6084-6090, doi: 10.1002/2015GL064650 (2015).

[30] Äijälä, M. et al. Constructing a data-driven receptor model for organic and inorganic aerosol: a synthesis analysis of eight mass spectrometric data sets from a boreal forest site. *Atmos. Chem. Phys.* **19**, 3645-3672 (2019).

[31] Eloranta, E.W. High Spectral Resolution Lidar in Lidar: Range-Resolved Optical Remote Sensing of the Atmosphere, Springer Series in Optical Sciences (Springer-Verlag, New York, 2005).

[32] Brenquier, J.L., Pawlowska, H. & Schüller, L. Cloud microphysical and radiative properties for parameterization and satellite monitoring of the indirect effect of aerosol on climate. *J. Geophys. Res.* **108**, 8632, doi:10.1029/2002JD002682 (2003).

[33] Gettelman, A. Putting the clouds back in aerosol-cloud interactions. *Atmos. Chem. Phys.* **15**, 12397-12411 (2015).

[34] Rosenfeld, D. et al. Satellite retrieval of cloud condensation nuclei concentrations by using clouds as CCN chambers. *Proc. Nat. Acad. Sci.* **113**, 5828-5834 (2016).

[35] Hoppel, W.A., Frick, G.M. & Larson, R.E. Effect of nonprecipitating clouds on the aerosol size distribution. *Geophys. Res. Lett.* **13**, 125-128 (1986).

[36] Covert, D.S., Kapustin, V.N., Bates, T.S. & Quinn, P.K. Physical properties of marine boundary layer aerosol particles of the mid-Pacific in relation to sources and meteorological transport. *J. Geophys. Res.* **101**, 6919-6930 (1996).

[37] Andronache, C. Estimated variability of below-cloud removal by rainfall for observed aerosol size distributions. *Atmos. Chem. Phys.* **3**, 131-143 (2003).

[38] Pryor, S.C., Joerger, J.M. & Sullivan, R.C. Empirical estimates of size-resolved precipitation scavenging coefficients for ultrafine particles. *Atmos. Environ.* **143**, 133-138 (2016).

[39] Bollasina, M.A., Ming, Y. & Ramaswamy, V. Anthropogenic aerosols and the weakening of the South Asian summer monsoon. *Science* **334**, 502-505 (2011).

[40] Coopman, Q., Garrett, T.J., Finch, D.P. & Riedi, J. High sensitivity of Arctic liquid clouds to long-range anthropogenic aerosol transport. *Geophys. Res. Lett.* **45**, 372–381 (2018).

[41] Brient, F. & Bony, S. Interpretation of the positive cloud feedback predicted by a climate model under global warming. *Clim. Dyn.* **40**, 2415-2431 (2013).

[42] Teuling, A.J. et al. Observational evidence for cloud cover enhancement over western European forests. *Nature Comm.* **8**, 14065 (2017).

Methods

SMEAR II station. The Station for Measuring Ecosystem – Atmosphere Relations (SMEAR II[28]) station at Hyytiälä (61°51'N, 24°17'E, 180 m above sea level) has extensive facilities for measuring forest-atmosphere relations and has been active since 1996. This site is the flagship of the SMEAR network providing, for example, the longest continuous time series of sub-micron aerosol number size distribution measurements. The main research fields are: analysis of gas and particle concentrations and fluxes and their role in aerosol and cloud formation; analysis of water, carbon and nutrient budgets of the forested catchment, and analysis of environment and tree structure on gas exchange, water transport and growth of trees.

http://www.atm.helsinki.fi/SMEAR/index.php/smear-ii

BAECC campaign. Biogenic Aerosols – Effect on Clouds and Climate (BAECC) was an intensive 8-month campaign in Hyytiälä, Finland, where the U.S. Department of Energy (DOE)'s Atmospheric Radiation Measurement (ARM) Program deployed their Second ARM Mobile Facility (AMF2). The AMF2 was operational from February to September 2014. The AMF2 included in-situ aerosol instruments as well as a suite of ground-based remote sensing instruments. The campaign aims[43] and the observational capacity and initial results[25] are presented elsewhere.

In-situ instrumentation

DMPS. The aerosol number size distribution was measured with Differential Mobility Particle Sizer (DMPS) for the size range from 3 nm to 1000 nm in electrical equivalent diameter. The DMPS is a twin-DMPS system[44] with a closed loop flow arrangement[45]. The time resolution for a full particle size distribution scan is 10 min. The instrument was operated following guidelines[46] from the Aerosols, Trace Gases, and Clouds Research Infrastructure (ACTRIS). The sample was drawn from 8 m height inside the canopy.

Nephelometer. The measurements of aerosol scattering and backscattering at the ground level were conducted at three wavelengths using an integrating nephelometer (TSI model 3563). The sample air is taken through a PM10 inlet (Digitel low volume inlet, DPM10/01/00/16) and alternating either directly to the instruments or via a PM1 impactor (Dekati PM impactor with a PM1 cut-off). The Nephelometer data was truncation corrected in accordance with the size cut of the impactor.[47]

Cloud Condensation Nuclei Counter (CCNC). The concentration of aerosol particles that activate in different supersaturations (Sc = 0.1 %, 0.2 %, 0.3 %, 0.5 % and 1.03%) with respect to water vapor was determined with Droplet Measurement Technologies Inc. Cloud Condensation Nuclei Counter[48]. The instrument sampled from the same inlet as the DMPS that extracted the sample from 8 m height inside the canopy.

Aerosol Chemical Speciation Monitor (ACSM). Submicron aerosol chemical composition was analyzed using the Aerosol Chemical Speciation Monitor[49]. In the ACSM, all non-refractory aerosol is vaporized and subsequently ionized using hard 70eV electron ionization (EI). A mass spectrum of the ions is then measured with a quadrupole mass

analyzer. Organic aerosol sub-species (semi-volatile and low volatile organic aerosol classes; SV-OOA and LV-OOA) were de-convolved from the data using Positive Matrix Factorization[50] (PMF).

High Spectral Resolution Lidar (HSRL). Vertical profiles of optical depth, backscatter cross-section, depolarization and backscattering coefficients were determined with HSRL[51]. As an internal calibration, molecular scattering was used as a refence at each point of the lidar profile. More details can be found from[31]. The instrument was operated as part of AMF2 facility[52].

Radiosoundings. Meteorological radiosonde soundings[53] were performed 4 times per day during the campaign. Relative humidity, air temperature and pressure readings from radiosondes were used to calculate specific humidity at the levels of 200, 500 and 1000 m above ground level. Additionally, specific humidity near the surface (4 m above ground) was estimated from near-surface measurements.

Weather Sensor. Vaisala FD12P weather sensor located at 18 m height provided data on precipitation amount. The AMF2 provided additional supporting in-situ weather parameters[54].

Cloud observations

CEILOMETER. Vaisala CL31 was used to derive cloud base height[55].

MWACR. W-Band vertically pointing Doppler cloud radar operating at 95.04 GHz provided data on reflectivity that was used in the cloud properties retrieval scheme[56].

Microwave radiometer. Column-integrated liquid water path content was measured with a microwave radiometer (MWR[57]). MWR operates at two frequencies: 23.8 and 31.4 GHz. Integrated liquid water path is derived from radiance measurements with a statistical retrieval algorithm that uses monthly derived and location-dependent linear regression coefficients. MWR provides data in cm that is converted to g m^{-2}.

Cloudnet. The Cloudnet target classification product[58] that provides information on cloud and hydrometeor types as well as cloud boundaries was used to select cases for CDNC retrieval. The cloud fraction product was also used in the analysis[59].

Satellite retrieval of Cloud Condensation Nuclei. The satellite retrieval of CCN is based on the methodology of Rosenfeld et al[34]. More specifically, the satellite-retrieved adiabatic cloud drop concentrations (N_d) and cloud base updraft (W_b). The peak water vapor super saturation (S) near cloud base is calculated based on N_d and W_b. Nd is then by definition the CCN(S). The retrieval of CCN and S are mapped by an automatic procedure[60] for running windows of 36 x 36 km.

Data analysis and processing

Data coverage

The SMEAR II station was operational during the whole BAECC campaign while the AMF2 instruments operated only during the campaign, active between February 1 –

September 13, 2014. To harmonize the data used in the analysis, we compiled a specific campaign data set used in the analysis described in Extended Data Table 1.

Origin of measured air masses and selection of air mass transport sectors

For all of the data measured at the SMEAR II station, a 27-member ensemble of 96-h backtrajectories arriving hourly at 100 m a.g.l. was computed with the HYSPLIT model[61]. With the model, we used meteorological data files NCEP/GDAS with horizontal resolution 1°.[62] Ensemble mean trajectories were calculated. Ensemble mean trajectories that spent at least 90% of their time in the selected sector qualified to be further used in time-over-land analysis. The 90% criterion is aimed to minimize effect of adjacent sectors on passing air masses.

Three air mass transport sectors were considered in this work (see Fig. 1a in the main text), termed clean, studied and polluted transport sector. The clean sector is the same as that was used originally by Tunved et al.[17], representing air masses with minimal anthropogenic influence during the March-September period each year. In order to increase the number of data points related to cloud measurements, we extended the clean sector slightly to the east (See Figure 1a in the main text). The risk associated with this procedure is the potential contamination of measured air by anthropogenic activities in the Kola Peninsula area, known to influence atmospheric new particle formation and growth downwind from this area[63]. We found little difference between the clean and studied sector in terms of how the aerosol mass concentration or sub-100 nm particle size distribution evolves as a function of time over land (Figs. 1b, 2a, Extended Data Fig 8 and 9), which justifies the use of this extended transport sector in our analyses. Contrary to these two air mass transport sectors, measured aerosol properties are very different in the polluted sector (Extended Data Figs. 8-10).

Overall, between February 1 to September 31, 2014, there are 224 days with a total of 5376 ensemble trajectories. Out of this, there were 1342 trajectories that fulfilled the selection criteria for studied sector, 646 for the clean sector and 823 for the polluted sector. In percent, the coverage is therefore 24.9%,12.0% and 15.3%, for the studied, clean and polluted sectors, respectively.

The concept "time over land"

For each air mass back trajectory ensemble mean, we determined the time that this air had spent over a land area prior to its arrival at the SMEAR II station.

In the case of the studied (and clean) transport sector, the "time over land" has a very simple interpretation: it is the time that air originating from either Atlantic or Arctic Ocean spends over a boreal forest region before arriving at the measurement site SMEAR II. By plotting any measured quantity as a function of time over land, we show how this quantity, having initially a value typical for relatively clean marine air, is expected to evolve in time when being exposed to various sink and source processes associated with an atmospheric boundary layer over boreal forest.

In the case of the polluted sector, the situation is more complicated: the measured quantity does not necessarily correspond to originally clean marine air, in addition to which it may have been affected by anthropogenic emissions before being measured at SMEAR II.

Selection of cloud cases and Cloud Droplet Number Concentration (CDNC) retrieval

The Cloudnet target classification product was used to select suitable data for the study of cloud profiles. The Cloudnet target classification algorithm[59] utilizes cloud radar, lidar and microwave radiometer measurements to identify the presence and type of hydrometeors in the atmosphere. Warm non-precipitating clouds with cloud bases lower than 2000 m were selected for the analysis. A threshold of 2000 m was selected as a proxy for the mixing layer height to limit the number of cases where the cloud layer is decoupled from the surface. If drizzle / rain, the melting layer or ice crystals were present in the cloud profile, it was discarded from consideration. Multilayer cloud profiles were discarded from the analysis as well, however profiles containing ice clouds present aloft were retained if the distance between the warm cloud and the ice cloud was at least 1 km.

To derive cloud droplet number concentration (CDNC) the Frisch et al.[64] method was used. The method assumes the cloud droplet size distribution can be approximated by a gamma distribution with the fixed shape parameter[65]. It is also assumed that the CDNC is constant with height, which is one reason why our case selection was limited to non-precipitating, non-drizzling clouds. The retrieval uses measurements of LWP by MWR and radar reflectivity factor as given by MWACR. One of the major sources of uncertainties is the instrument calibration. The radar was cross calibrated against other radars operating on the site[66]. It should also be noted that the radar calibration during BAECC was rather stable[67]. The LWP observations follow ARM standard practices.

Data availability.

Measurement data for the analysis and figures in this study are archived on the Zenodo repository (doi:10.5281/zenodo.5645340). Source data is provided with this paper.

The SMEAR II data is available through avaa-portal (smear.avaa.csc.fi).

The ground-based data used in this article are generated by the Atmospheric Radiation Measurement (ARM) user facility and are made available from the ARM Data Discovery website (https://adc.arm.gov/discovery/) as follows:

ceilometer data (CEIL) from https://doi.org/10.5439/1181954,
dual-channel microwave radiometer (MWR) from https://doi.org/10.5439/1046211,
high spectral resolution lidar (HSRL) from https://doi.org/10.5439/1025200,
optical rain gauge (MET) from https://doi.org/10.5439/1786358,
W-band cloud radar (MWACR) from https://doi.org/10.5439/1150242.

The products derived from the ground-based remote-sensing data used in this article (target classification, cloud fraction, liquid water content) are generated by the European Research Infrastructure for the observation of Aerosol, Clouds and Trace Gases (ACTRIS) and are available from the ACTRIS Data Centre using the following link: https://hdl.handle.net/21.12132/2.c85c6a6c2bc348f8.

Code availability.

The codes for time over land calculations are available from the authors upon request. The CCN retrieval package can be obtained upon request from the first author of the following paper: Yue, Z., Rosenfeld, D., Liu, G., Dai, J., Yu, X., Zhu, Y., Hashimshoni, E., Xu, X., Hui, Y. and Lauer, O. (2019). Automated Mapping of Convective Clouds (AMCC) Thermodynamical, Microphysical and CCN Properties from SNPP/VIIRS Satellite Data. J. Appl. Met. Clim. https://doi.org/10.1175/JAMC-D-18-0144.

Methods references

[43] Petäjä, T. Science Plan: Biogenic Aerosols – Effects on Clouds and Climate (BAECC). US Department of Energy, Office of Science, DOE/SC-ARM-13-024 (2013).

[44] Aalto, P. et al. Physical characterization of aerosol particles during nucleation events. Tellus B, 53, 344-358 (2001).

[45] Jokinen, V. & Mäkelä, J.M. Closed loop arrangement with critical orifice for DMA sheath/excess flow system. *J. Aerosol Sci.* **28**, 643-648 (1997).

[46] Wiedensohler, A. et al. Mobility particle size spectrometers: harmonization of technical standards and data structure to facilitate high quality long-term observations of atmospheric particle number size distributions. *Atmos. Meas. Tech.* **5**, 657–685 (2012).

[47] Anderson, T.L. & Ogren, J.A. Determining aerosol radiative properties using the TSI 3563 integrating nephelometer. *Aerosol Sci. Technol.* **29**, 57-69 (1998).

[48] Paramonov, M. et al. A synthesis of cloud condensation nuclei counter (CCNC) measurements within the EUCAARI network. *Atmos. Chem. Phys.* **15**, 11999-12009 (2015).

[49] Ng, N.L. et al. An Aerosol Chemical Speciation Monitor (ACSM) for routine monitoring of the composition and mass concentrations of ambient aerosol. *Aerosol Sci. Technol.* **45**, 780–794 (2011).

[50] Paatero, P. & Tapper, U. Positive matrix factorization: A non-negative factor model with optimal utilization of error estimates of data values. *Environmetrics*, **5**, 111-126 (1994).

[51] Bambha, R., Eloranta, E., Garcia, J., Michelsen, H., Goldsmith, J., & Ermold, B. High Spectral Resolution Lidar (HSRL), 2014-02-01 to 2014-09-12, from the ARM Mobile Facility (AMF2, TMP) at the U. of Helsinki Research Station (SMEAR II), Hyytiala, Finland, https://doi.org/10.5439/1025200 (ARM, accessed 2014-10-13).

[52] Goldsmith, J. High Spectral Resolution Lidar (HSRL) instrument handbook. US Department of Energy, Office of Science, DOE/SC-ARM-TR-157 (2016).

[53] Atmospheric Radiation Measurement (ARM) user facility. 2014, updated hourly. Balloon-Borne Sounding System (SONDEWNPN). 2014-02-02 to 2014-09-12, ARM Mobile Facility (TMP) U. of Helsinki Research Station (SMEAR II), Hyytiala, Finland; AMF2 (M1). Compiled by D. Holdridge, J. Kyrouac and R. Coulter. ARM Data Center. Data set accessed May 2015 at http://dx.doi.org/10.5439/1021460.

[54] Kyrouac, J., & Shi, Y. Surface Meteorological Instrumentation (MET), 2014-02-01 to 2014-09-13, from the ARM Mobile Facility (AMF2, TMP) at the U. of Helsinki Research Station (SMEAR II), Hyytiala, Finland, https://doi.org/10.5439/1786358, (ARM, accessed 2014-10-13).

[55]Morris, V., Zhang, D., & Ermold, B. Ceilometer data (CEIL), 2014-02-01 to 2014-09-13, from the ARM Mobile Facility (AMF2, TMP) at the U. of Helsinki Research Station (SMEAR II), Hyytiala, Finland, https://doi.org/10.5439/1181954 (ARM, accessed 2014-10-13).

[56] Lindenmaier, I., Bharadwaj, N., Johnson, K., Isom, B., Hardin, J., Matthews, A., Wendler, T., & Castro, V. Marine W-Band (95 GHz) ARM Cloud Radar (MWACR), 2014-02-01 to 2014-09-13, from the ARM Mobile Facility (AMF2, TMP) at the U. of Helsinki Research Station (SMEAR II), Hyytiala, Finland, https://doi.org/10.5439/1150242 (ARM, accessed 2014-10-13).

[57] Cadeddu, M. Microwave Radiometer (MWRLOS), 2014-02-01 to 2014-09-13, from the ARM Mobile Facility (AMF2, TMP) at the U. of Helsinki Research Station (SMEAR II), Hyytiala, Finland, https://dx.doi.org/10.5439/1046211 (ARM, accessed 2014-10-13).

[58] Cloud profiling products: Classification, Liquid water content, Categorize; 2014-02-02 to 2014-09-09; from Hyytiälä. Generated by the cloud profiling unit of the ACTRIS Data Centre, https://hdl.handle.net/21.12132/2.c85c6a6c2bc348f8 (ACTRIS, accessed 2017-09-01.

[59] Illingworth, A.J. et al. (2007) Cloudnet: Continuous Evaluation of Cloud Profiles in Seven Operational Models Using Ground-Based Observations, *Bull. Am. Met. Soc.* **88**, 883-898.

[60] Yue, Z. et al. Automated mapping of convective clouds (AMCC) thermodynamical, microphysical and CCN Properties from SNPP/VIIRS satellite data. *J. Appl. Met. Clim.* https://doi.org/10.1175/JAMC-D-18-0144.1 (2019).

[61] Stein, A.F. et al. NOAA's HYSPLIT atmospheric transport and dispersion modelling system, *Bull. Am. Met. Soc.* **96**, 2059-2077 (2015).

[62] Kanamitsu, M. Description of NMC global data assimilation and forecast system, *Weather Forecast.* **4**, 335-342 (1989).

[63] Kyrö, E.-M. et al. Trends in new particle formation in Eastern Lapland, Finland: effect of decreasing sulfur emissions from Kola Peninsula, *Atmos. Chem. Phys.* **14**, 4383-4396 (2014).

[64] Frisch, S., Shupe, M., Djalalova, I., Feingold, G. & Poellot, M. The retrieval of stratus cloud droplet effective radius with cloud radars, *J. Atmos. Ocean. Tech.*, **19**, 835-842 (2002).

[65] Sarna, K. & Russchenberg, H.W.J. Ground-based remote sensing scheme for monitoring aerosol–cloud interactions, *Atmos. Meas. Tech.* **9**, 1039-1050 (2016).

[66] Falconi, M.T., von Lerber, A., Ori, D., Marzano, F.S. & Moisseev, D. Snowfall retrieval at X, Ka and W bands: consistency of backscattering and microphysical properties using BAECC ground-based measurements, *Atmos. Meas. Tech.* **11**, 3059-3079 (2018).

[67] Kollias, P., Puigdomènech Treserras, B. & Protat, A. Calibration of the 2007–2017 record of ARM Cloud Radar Observations using CloudSat, *Atmos. Meas. Tech.* **12,** 4949-4964.

[68] Canonaco, F., Crippa, M., Slowik, J.G., Baltensperger, U. & Prévôt, A.S.H. SoFi, an IGOR-based interface for the efficient use of the generalized multilinear engine (ME-2) for the source apportionment: ME-2 application to aerosol mass spectrometer data, *Atmos. Meas. Tech.* **6**, 3649-3661 (2013).

[69] Canagaratna, M.R. et al. Elemental ratio measurements of organic compounds using aerosol mass spectrometry: characterization, improved calibration, and implications, *Atmos. Chem. Phys.* **15**, 253-272 (2015).

740 [70] Crippa, M. et al. (2014) Organic aerosol components derived from 25 AMS datasets
741 across Europe using a newly developed ME-2 based source apportionment strategy.
742 *Atmos. Chem. Phys.* **14**, 6159-6176.

Supplementary Data Tables and Captions.

Supplementary Data Table 1. Instrument specific start and end dates (dd.mm.yyyy) for the data that was included in the analysis.

Instrument/dataset	Start date	End date
DMPS	01.04.2014	30.09.2014
Nephelometer	01.04.2014	30.09.2014
CCNC	01.04.2014	30.09.2014
ACSM	01.04.2014	30.09.2014
HSRL	01.04.2014	12.09.2014
Precipitation	01.04.2014	30.09.2014
Cloudnet target classification	01.04.2014	09.09.2014
MWACR	01.04.2014	13.09.2014
MWR	01.04.2014	12.09.2014
Radiosoundings	01.04.2014	12.09.2014
Cloudnet cloud fraction	01.04.2014	31.08.2014

Extended Data Figures and Figure Captions.

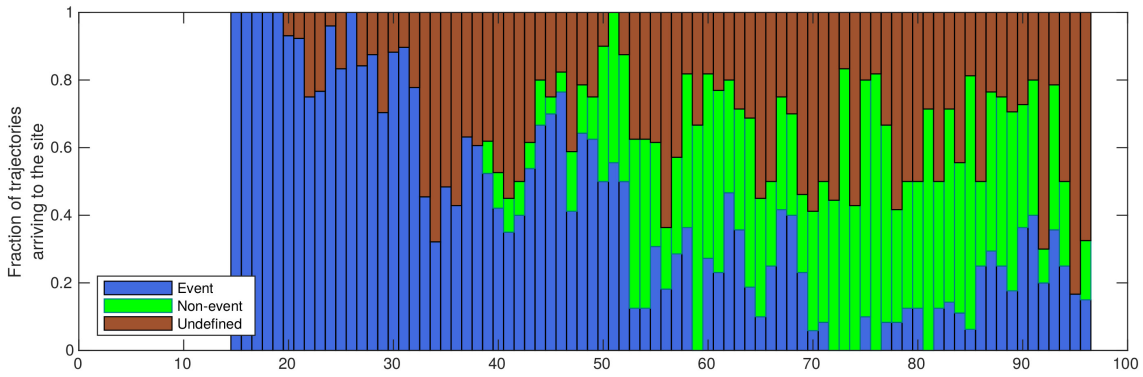

Extended Data Fig. 1. Statistics on events, non-events and undefined days as a function of time over land in the studied transport sector. Shorter air mass transport times over the boreal forest favor atmospheric new particle formation, whereas non-event days become more frequent at longer air mass transport times over land.

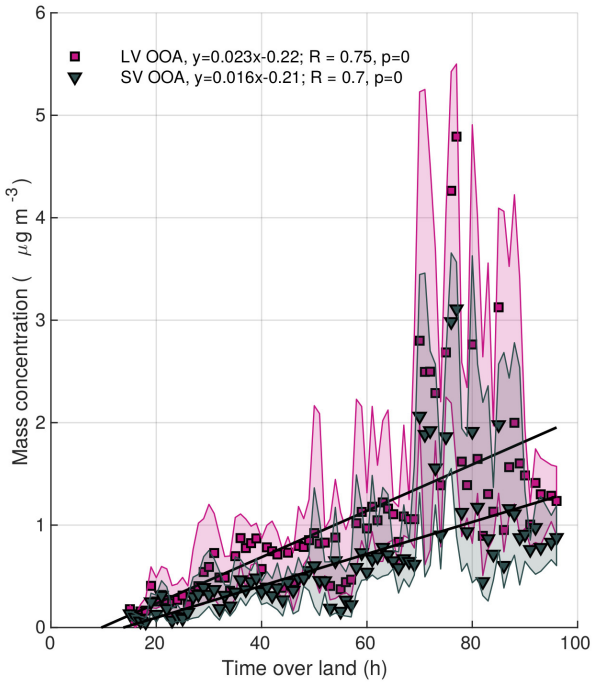

Extended Data Fig. 2. Organic aerosol composition as a function of time over land. A two-factor Positive Matrix Factorization (PMF[50]) solution performed with Source Finder (SoFi[68]) hints towards a large contribution of low-volatility oxygenated organic aerosol (LV-OOA) to the total organic loading. The oxidized CO_2^+ fragment contributes greatly to the LV-OOA mass concentration indicating a high degree of oxidation[69]. The semi-volatility oxygenated organic aerosol (SV-OOA) shows slightly lower loading compared to LV-OOA. We acknowledge that the PMF solution presented here only gives a rough estimate of the OA factors since also other factors, such as hydrocarbon-like organic aerosol (HOA) and biomass burning organic aerosol (BBOA) can contribute to the total organic loading. However, previous studies suggest that their contribution to the total organic aerosol is minor at SMEAR II as shown in Crippa et al[70]. Moreover, their finer separation would not change the LV-OOA loading due to the minor CO_2^+ ion fragment contribution to the HOA and BBOA mass spectra.

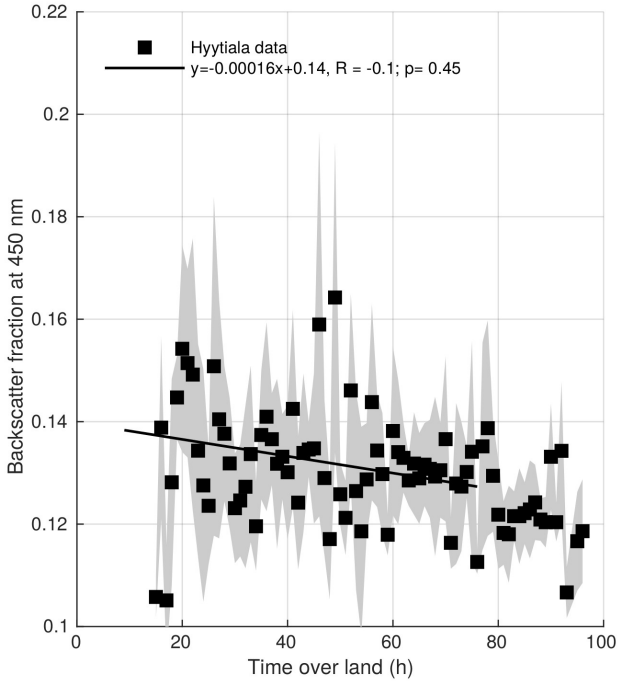

774

775

776 **Extended Data Fig. 3. Backscatter fraction as a function of time over land.** The
777 fraction of radiation scattered in the backward direction determined with the
778 nephelometer for the in-situ aerosol decreases as a function of time over land in the
779 studied transport sector. The figure shows that the aerosol particles grow to larger sizes
780 and thus scatter less into the backward direction as the air masses reside longer over the
781 boreal forest region.

782

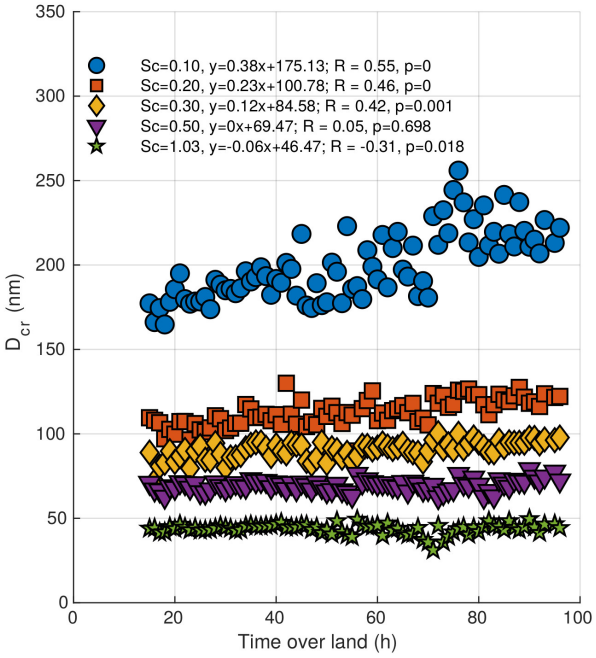

Extended Data Fig. 4. In-situ determined CCN activation diameters as a function of time over land. The critical CCN activation diameters at water vapor supersaturations (S_c) of 0.1 %, 0.2 %, 0.3 %, 0.5 % and 1.0 % as a function of time over land in the studied transport sector. Compared with sub-100 nm particles, the sub-population of particles able to act as CCN at S_c = 0.1% shows a notable increase D_{cr} as a function of time over land. This feature can be explained by a combination of two things: 1) these particles are aged, possibly originating from anthropogenic sources, making them relatively hygroscopic when entering the boreal forest region, 2) accumulation of rather non-hygroscopic organic vapors into these particles decreases their hygroscopicity with increasing transport times over the boreal forest.

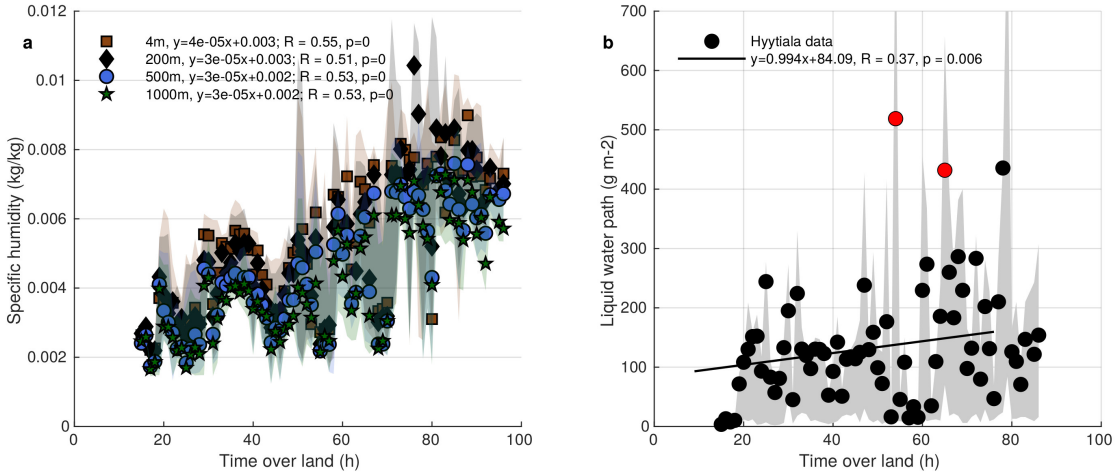

795 **Extended Data Fig. 5. a. Specific humidity and b. cloud liquid path (LWP) as a**
796 **function of time over land in the studied transport sector.** The data for time over land
797 < 75 h are used in the fitting and the two red points are removed from the fit as outliers.
798 The shaded areas show 25th and 75th percentiles that illustrate variability of measurements
799 contributing to the averaged LWP for a given time over land and are consistent with the
800 approach applied to creation of all other figures in the study.
801

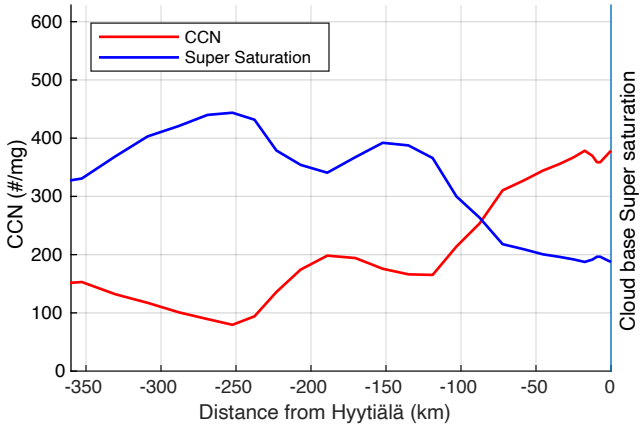

802
803 **Extended Data Fig. 6. Satellite derived CCN concentration along a selected trajectory.**
804 The trajectory arrived to Hyytiälä from the clean sector during August 17, 2014.
805
806

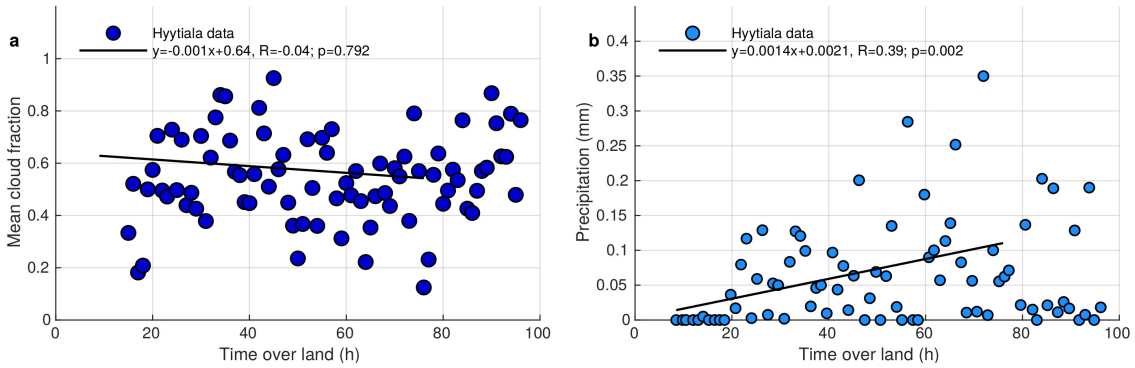

Extended Data Fig. 7. Cloud fraction and precipitation as a function of time over land. **a.** Mean cloud fraction as a function of time over land in the studied transport sector. **b.** Precipitation accumulated in the hour following trajectory arrival to the station as a function of time over land in the studied transport sector. There is an outlier at (78 h; 1 mm) not shown in the figure, corresponding to a single heavy rain event.

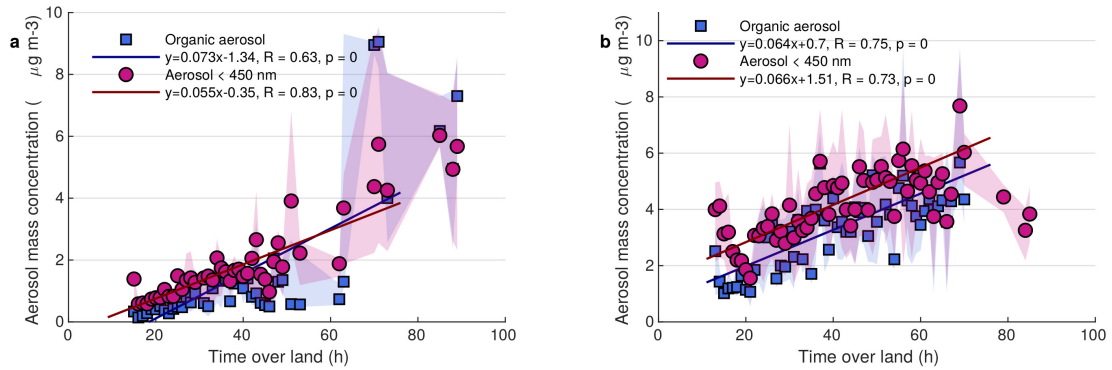

Extended Data Fig. 8. Time evolution of the total particle mass concentration and organic aerosol mass concentration in different air mass sectors. The same as Fig 2a, but **a.** clean and **b.** polluted air mass transport sectors.

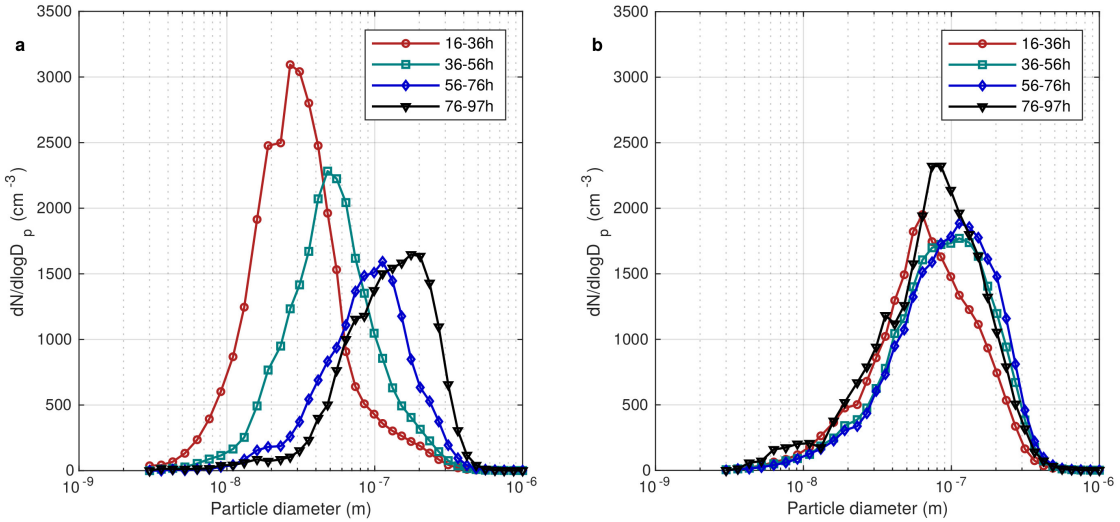

Extended Data Fig 9. Time evolution of the particle number size distribution. The same as Figure 1c, but **a.** the clean and **b.** polluted air mass transport sectors.

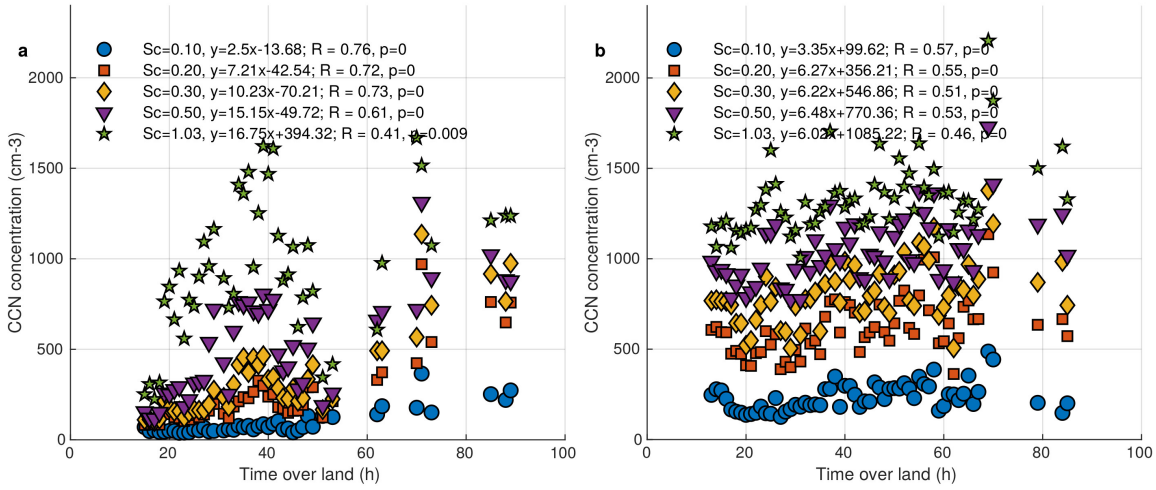

Extended Data Fig 10. Cloud-related variables. The same as Figure 3a, except for **a.** the clean and **b.** polluted air mass transport sectors.